The Influence of Drying-Wetting Cycles on the Suction Stress of Compacted Loess and the associated Microscopic Mechanism

Yongpeng Nie
Chang'an University
Wan kui Ni (niwankui@chd.edu.cn)
Chang' An University https://orcid.org/0000-0001-5296-4045
Xiangning Li
Chang'an University
Haiman Wang
Chang'an University
Kangze Yuan
Chang'an University
Wenxin Tuo
Chang'an University

Research Article

Keywords: Compacted loess, Drying-wetting cycles, Suction stress characteristic curve, Microstructure, Pore Size Distribution, New computational model

Posted Date: March 23rd, 2021

DOI: https://doi.org/10.21203/rs.3.rs-317088/v1

The Influence of Drying-Wetting Cycles on the Suction Stress of Compacted Loess and the associated Microscopic Mechanism

Yongpeng Nie[a,b], Wankui Ni[a,b]*, Xiangning Li[a,b], Haiman Wang[a,b], Kangze Yuan[a,b], Wenxin Tuo[a,b]

* Corresponding author (Wankui Ni, Email address: niwankui@chd.edu.cn)

[a] School of Geology Engineering and Geomatics, Chang'an University, Xi'an, Shaanxi 710054, P.R. China

[b] Key Lab of Western Geological Resources and Geoengineering under Ministry of Education, Chang'an University, Xi'an, Shaanxi 710054, P.R. China

Abstract

In order to better understand and analyze the unsaturated stability of loess fillings, it is necessary to study the changes in suction stress before and after the drying-wetting cycles. In this study, the soil-water characteristic curve (SWCC) of compacted loess before and after drying-wetting cycles was tested using the filter paper method. Then, the suction stress was calculated and the microstructure of the loess sample was determined by the scanning electron microscope（SEM）and nuclear magnetic resonance (NMR). The results showed that the drying-wetting cycles had an important influence on the suction stress characteristic curve (SSCC) and microstructure of compacted loess. The change in suction stress before and after the drying-wetting cycles can be explained by the loess microstructure. The drying-wetting cycles did not significantly change the basic trend of the compacted loess's suction stress, but it increased the porosity and the diameter of the dominant pore (i.e., the inter-aggregate pore) of the sample, and reduced the suction stress when the same matrix suction was applied. The main significant change in suction stress with matrix suction occurred within the range of the dominant soil pores. The larger the diameter of the dominant pore, the smaller the suction stress under the same matrix suction. In addition, this study also proposes a new method for calculating suction stress based on the pore size distribution（PSD）parameters, which is more convenient than traditional calculation methods based on SWCC parameters.

Keywords: Compacted loess; Drying-wetting cycles; Suction stress characteristic curve; Microstructure；Pore Size Distribution；New computational model

1. Introduction

Loess is a silty yellow sediment formed in the Quaternary period that was gradually transported and accumulated during a long geological age (Peng et al. 2018; Peng et al. 2017). It is widely distributed in China and is mainly concentrated in the Yellow River, the upper reaches of Shanxi, Shaanxi, southeastern Gansu, and western Henan, as well as other arid and semi-arid areas, covering an area of 640,000 km^2 and accounting for about 6% of China's total land area (Derbyshire 2000; Feng et al. 2015; Luo et al. 2017; Ni et al. 2020). At present, with the implementation and advancement of China's "Western Development" strategy, more and more infrastructure projects are being constructed in the Loess Plateau (Feng et al. 2015). Local materials are usually used for construction, and the loess is compacted as the filling material in roadbed slopes (Qin et al. 2020). However, variable rainfall intensity, changes in groundwater, and surface evaporation in the Loess Plateau created a regular dry-moist cycle in local soils. These climatic changes cause the drying-wetting cycles to occur under natural conditions, which affects soil hydraulic properties (Kong et al. 2017) and shear strength (Li et al. 2018), important factors which influence the fill and loess slope stability.

At the same time, loess has very complex soil-water and engineering characteristics in an unsaturated state (Zhang et al. 2020). In general, most unsaturated slopes tend to lose stability during the process of seepage or when water pressure rises in soil pores (Lourenco et al. 2015; Schnellmann et al. 2010). Water infiltration causes a decrease in the suction of unsaturated soil, but the increase in pore water pressure when the groundwater level rises reduces the anti-slip force on the potential slip surface, which may unbalance the slope and cause slip damage (Fredlund and Rahardjo 1993). To improve the bearing capacity and stability of unsaturated slopes in actual engineering construction, an in-depth understanding of the mechanical properties, seepage properties, and physical interface characteristics of unsaturated soils is needed (Collins and Znidarcic 2004).

An active point of study in modern soil mechanics concerns the properties and engineering characteristics of unsaturated soils. Many experiments and theoretical analyses have been done as early as the 1950s to better clarify the relationship between suction and effective stress or shear strength of unsaturated soil (Bishop and Blight 1963; Fredlund and Morgenstern 1978; Khalili and Khabbaz 2015; Vanapalli et al. 1996). Two general methods have been used to clarify the characteristics of unsaturated soils: the effective stress method proposed by Bishop (1959), and the independent state variable method proposed by Fredlund and Morgenstern (1978), both of which are difficult to apply to a large range of matric suction and unsaturated soil parameters. To further characterize and evaluate the influence of suction on the stress and shear strength of unsaturated soils, Lu and Likos (2006) proposed the concept of suction stress, which is a combination of negative pore water pressure and surface tension. The relationship between the net-grain force generated in the soil particle framework, the suction stress, and the matrix suction or effective saturation can be represented using the suction stress characteristic curve (SSCC), which describes the microscopic stress state of unsaturated soil. This method has a clearer physical meaning and is more in line with actual observations of unsaturated soils. Song (2012) estimated and compared the SSCC of sand and silt based on SWCC data and analyzed the influence of different relative densities on the evolution of sand SSCC (Song 2014). Oh et al. (2012) conducted a series of shear strength and soil moisture retention tests on several residual soils, discussed the essential relationship between SSCC and SWCC, and found that SSCC corresponds well to SWCC. In addition, Oh et al. (2013) provided an alternative method for obtaining SSCC through a triaxial K_0 consolidation test on granite residual soil, further proving the effectiveness of SSCC in describing the consolidation and shear strength characteristics of unsaturated soils. Jiang et al. (2016) found that SSCC varies significantly with different dry densities and soil water content based on loess SWCC data. Song and Hong (2020) compared the modified SSCC of granite and mudstone soils and concluded that the mineral composition and particle size distribution of unsaturated soil has a significant impact on its characteristics.

Our review of decades of research covering the definition and development of suction stress and SSCC found that most of the current research is limited to the initial soil state (such as density, water content, or mineral content). However, the understanding of the influence of external conditions on SSCC is incomplete. In particular, there is a lack of research on the influence of drying-wetting cycles on the suction stress of unsaturated compacted loess.

To address this knowledge gap, this paper studies the change law and mechanism of the SSCC of unsaturated compacted loess with different dry densities before and after drying-

wetting cycles. First, we used the filter paper method to measure the matrix suction and volumetric water content of unsaturated compacted loess before and after drying-wetting cycles, then used the VG model to fit the SWCC based on the test results, and then calculated the corresponding suction stress using the fitted SWCC parameters. Finally, we qualitatively and quantitatively analyzed the influence of drying-wetting cycles on the suction stress of unsaturated compacted loess by combining previous results with scanning electron microscope (SEM) and nuclear magnetic resonance (NMR) analysis on compacted loess samples. Based on the PSD parameters obtained using NMR, a new model to calculate suction stress was proposed.

2. Materials and methods

2.1 Materials

Loess samples used in this study were from Yan'an City, Shaanxi Province, China. Figure 1 is a schematic diagram of the main distribution locations and sampled locations. Samples were taken from Q_3 loess at a depth of 3m below the surface. The specific sampling process is as follows: after the sampling point is determined, the surface soil is removed, the sample is manually obtained from a depth of 3m to reduce disturbance, and the sample is carefully cut into a soil column with a diameter of 10cm and a height of 20cm, which is immediately put into the sampling cylinder, stored in bubble film, and transported back to the laboratory on the same day. The basic physical properties of the loess samples were measured according to ASTM 2006 Standard Test Methods (ASTM 2006), as shown in Table 1. The particle group analysis was performed with the Bettersize 2000 laser particle size tester. The results showed that the loess sample was mainly composed of silt (about 90.04%) and clay particles (about 9.96%) (Table 1 and Figure 2).

Fig. 1 should be here

Table 1 should be here

Fig. 2 should be here

2.2 Sample preparation

A proper amount undisturbed soil from a depth of 3m was crushed until all visible aggregates were destroyed, then placed in a thermostat at 105°C and dried. The dry loess was then passed through a 2mm sieve, sprayed with distilled water until the water content reached 10% and stirred, then put in a plastic bag and stored for 48h to achieve sample moisture balance. Next, soil samples were weighed corresponding to the target dry density (1.45g/cm^3, 1.55g/cm^3 and 1.65g/cm^3), put into a mold with a diameter of 61.8mm and a height of 20mm, and then statically compacted at a constant displacement rate of 0.4mm/min, at which point they were taken out of the mold. The loess samples used in this study were all prepared using this method.

2.3 Drying-wetting cycles

Since the soil structure can reach an equilibrium state after three cycles of wetting and drying(Al-Homoud et al. 1995), we fixed the observed number of drying-wetting cycles to three in this study. Due to rainfall infiltration, ground water level change, or evaporation caused by the migration of natural moisture in the soil mass approximation for one dimension (Liu 2011), we tried to accurately simulate the natural conditions of the dry-wet cycle circulation and humidifying process using the water film transfer method: by evenly and slowly dropping the

required amount of water on the surface of the sample until saturation, then air drying to 10% moisture content. This process was repeated for three wet and dry cycles.

2.4 Microstructural Investigation

To observe the microstructure of the samples, NMR and SEM tests were performed on the samples before and after the drying and wetting cycles.

2.4.1 NMR tests

A nuclear magnetic resonance analyzer (PQ-001) was used to test the distribution curve of relaxation time (T2) of compacted loess samples before and after drying-wetting cycles with different dry densities. The specific operation steps were defined as in Tian et al. (2014).

Since the distribution of relaxation time has a linear relationship with the aperture distribution curve (PSD), according to the distribution of relaxation time, the PSD of the drying-wetting cycles pattern can be calculated by Equation (1) (Kleinberg and R. 2003).

$$\frac{1}{T_2} = \rho_2 \frac{4}{D} = \sqrt{\frac{k_s}{\emptyset^4 T_{2LM}^2}} \frac{4}{D} \tag{1}$$

where D is pore diameter(um); ρ_2 is the transverse surface relaxation intensity (um/ms); k_s is the saturated permeability of the soil; $\emptyset$ is porosity; and T_{2LM} is the geometric mean of the T_2 distribution.

Using a dry density of 1.45g/cm³ as an example, k_s is 1.18×10^{-13} m^2; $\emptyset$ is 0.49; T_{2LM} is 0.52989 ms, so ρ_2 is 2.69 um/ms. Substituting the obtained ρ_2 into equation (1), the T2 curve can be converted into a pore size distribution curve. The pore size distribution curves in this study are all converted from the T2 curve using this method.

2.4.2 SEM tests

After completing the nuclear magnetic resonance test, a scanning electron microscope (Quanta 200FEG) was used to scan the compacted loess samples before and after the drying-wetting cycles at different dry densities to obtain microstructure photos. The specific operation steps were defined as in Ni et al. (2020).

2.5 SWCC test

In this study, the SWCC of the compacted loess sample was measured using the filter paper method (Whatman No. 42). Using two samples as a set, a small amount of distilled water was dopped evenly and slowly onto the surface of the sample using different pre-prepared water contents ranging between 10% and saturation. The water was distributed evenly, then carefully sealed with plastic wrap and stored in a moisturizer. After three days, an ear ball was used to remove the surface of the topsoil, then a protective filter paper, test filter paper and another protective filter paper layer were placed on the top of the sample. Another sample from the same group was then layered on top of it, pressed together, and sealed with insulating tape. Finally, the samples were sealed with insulating film and transparent tape and placed in an incubator at 30℃ for 10 days. After 10 days, water exchange was completed between the soil sample and the filter paper. The sealed sample was quickly separated, and the test filter paper was carefully and rapidly weighed with a high-precision analytical balance (0.0001g) within five seconds to measure its water content. The matric suction was calculated according to the water content of the filter paper (ASTM 2013). According to this method, the SWCC of loess

samples before and after the drying-wetting cycles at different dry densities can be obtained.

3. Results and discussion

3.1 SWCC

The laws of soil and water movement are complex, and it is very difficult to use theoretical methods to derive their exact expressions (Leong and Rahardjo 1997). Therefore, many scholars have created empirical formulas based on a large number of experiments to describe the laws of soil and water migration (Fredlund and Xing 1994; Genuchten and Th. 1980). Among the many SWCC models, the VG model (Equation 2) has higher accuracy for fine-grained soils (such as loess) (Sommer and Stoeckle 2010), and was used in this study to analyze the compacted loess samples obtained.

$$S_e = \frac{\theta - \theta_r}{\theta_s - \theta_r} = \left[\frac{1}{1 + (a\psi)^n}\right]^{1-\frac{1}{n}} \quad (2)$$

In the formula, S_e is effective saturation; θ is volumetric water content; θ_r is residual volumetric water content; θ_s is saturated volumetric water content; ψ is matrix suction; and a and n are fitting parameters, where a is related air enter value (AEV), and n reflects the shape of SWCC.

Least squares optimization and the nonlinear curve fitting algorithm were used to fit the matrix suction and volumetric water content obtained experimentally according to the VG model. Specific values of the fitting parameters were obtained, and the AEV was determined according to the quantitative method proposed by Zhai and Rahardjo (2012). The results are shown in Table 2.

Table 2 should be here

SWCC comparisons from compacted loess samples before and after different dry densities and drying-wetting cycles are shown in Figure 3. It can be seen from the figure that as the dry density increases, SWCC gradually becomes steeper. The slope of SWCC reflects the rate of change of moisture content with substrate suction: the greater the slope, the faster the moisture content changes with substrate suction, and the faster the rate of soil moisture loss. The change in SWCC slope indicates that the volumetric water content of the low-density loess sample has a large change, the matrix suction has a small change, and the water holding capacity is weaker. In addition, the SWCC of the three loess samples crossed when the matrix suction was about 18kPa and the volumetric water content was about 35%, defined as the critical water content or critical matrix suction. Before the intersection, the sample with a low dry density maintained a higher volumetric water content, while after the intersection, the sample with a higher dry density maintained a higher volumetric water content. The SWCC cross phenomenon shows that despite variations in the dry density of compacted loess, there is always a critical point at which loess of different dry densities have the same volumetric water content and matrix suction. This critical point is only affected by the particle size, not the particle spacing (Xie et al. 2020).

The saturated volumetric water content reflects the total pore volume of the soil and the AEV reflects the large pore volume of the soil (Burger and Shackelford 2001). After the samples with different dry densities underwent the drying-wetting cycles, the saturated volumetric water content increased while the AEV decreased (Figure 3b-c, Table 2), indicating that the soil

porosity and macropore volume both increased under the action of dry and wet cycles. For the compacted loess samples, the volume of the soil macropores before the drying-wetting cycles was relatively small, resulting in a higher AEV; on the contrary, the drying-wetting cycles produced larger pores, resulting in a decrease in the AEV. Compared with the other two dry density samples, the sample with a dry density of 1.45g/cm^3 had the smallest change in SWCC morphology before and after the drying-wetting cycles, indicating that the drying-wetting cycles weakly impacted the porosity of the sample at this density. As dry density increased, the SWCC morphology changes before and after the drying-wetting cycles became increasingly obvious, indicating that the influence of drying-wetting cycles on SWCC increased with an increase in dry density.

Fig. 3 should be here

3.2 SSCC

Two methods can be used to obtain soil suction stress: a triaxial test or SWCC parameter estimation, but the difference between the two results is only a dozen kPa (Lu et al. 2010; Oh et al. 2012), and the impact of the difference in the results on subsequent studies is negligible. Therefore, in consideration of the convenience of obtaining the SSCC of compacted loess samples and to better understand the influence of drying-wetting cycles on the soil-water system, SWCC parameters based on patterns from compacted loess were used to calculate the suction stress.

From equation (3) (Lu and Likos 2004), the suction stress σ^s is a function of the effective saturation S_e, and there is a one-to-one correspondence between the saturation and the matrix suction in the soil. Therefore, in equation (4), we use SWCC's VG model to express the relationship between matrix suction and suction stress.

$$\sigma^s = -\psi S_e = -\psi \frac{\theta - \theta_r}{\theta_s - \theta_r} \tag{3}$$

$$\sigma^s = -\psi \left[\frac{1}{1 + (a\psi)^n}\right]^{1-\frac{1}{n}} \tag{4}$$

According to Equations (3) and (4), we can get the relationship curve of suction stress and matric suction of compacted loess at different dry densities before and after the wetting cycle, generating the suction stress characteristic curve (SSCC), as shown in Figure 4. It was found that the SSCC was non-linear, and each SSCC had a turning point near the AEV. This meant that when the matric suction was less than the AEV, the suction stress of the sample increased sharply with the matric suction; however, when the matric suction was greater than the AEV, the suction stress was constant with increasing matric suction. The relationship in which suction stress increases sharply with matric suction and then stabilizes is typical for the morphology of silty soil (Song and Hong 2020). However, the basic morphology of the SSCC of the samples did not change significantly due to the drying-wetting cycles (Figure 4b-c), indicating that the drying-wetting cycles did not change the particle composition of the compacted loess. At the same time, the SSCC can be divided into two different states according to the value of n (Lu 2004): when the value of n is less than or equal to 2.0, the suction stress monotonically increases and converges; when the value of n is greater than 2.0, the suction stress first increases and then decreases. By combining Figure 4 and Table 2, we know that the shape of SSCC depends on the value of n in the SWCC.

Although the basic form of SSCC was not significantly affected by dry density and the wet-dry cycle, as the dry density of the sample increased, the SSCC shifted upward as a whole, while the SSCC after the wet-dry cycle shifted downward as a whole. Under the same matrix suction, the specimen with higher dry density has the higher suction stress, while after the wet-dry cycle it has a lower suction stress. Considering that compaction and drying-wetting cycles can change the pore distribution in soil (Azizi et al. 2019), the phenomenon of SSCC changing with dry density and drying-wetting cycles can be explained as the influence of soil microstructure on the absorption stress of the sample.

The higher the dry density of the compacted loess sample, the higher the degree of compactness of the sample and the smaller the distance between particles, which increases the van der Waals forces and other physical interactions between the particles. The suction stress characterizes the interaction force between the particle layers. Therefore, the effect of dry density on suction stress is comprehensively reflected in changes of the sample density and enhanced Van der Waals forces so that the suction stress increases with the dry density.

Comparing the SSCC changes of the samples before and after the drying-wetting cycles under different dry densities (Figure 4b-c), we found that the SSCCs of the dry density (1.45g/cm^3) sample almost overlap, indicating that under the same matrix suction, the reduction in suction stress was very weak. As the dry density increased from 1.45g/cm^3 to 1.65g/cm^3, the downward shift of the SSCC after the drying-wetting cycles also increased, meaning that the attenuation of the suction stress increased and that the influence of dry-wet circulation on SSCC increased with dry density. This is similar to the change in SWCC, from which we can infer that the drying-wetting cycles have a more significant impact on the pore structure of high-pressure compacted loess samples than that of low-pressure compacted samples.

Fig.4 should be here

3.3 Microscopic analysis of changes in the suction stress of compacted loess samples

Soil pore characteristics (such as pore size, pore distribution) significantly affect the shape of SWCC (Ng et al. 2019). A closed model established based on SWCC parameters determines the values, and our analysis of SWCC test results demonstrates that the drying-wetting cycles cause obvious changes in the pore characteristics of compacted loess samples. Therefore, we have reason to believe that the drying-wetting cycles will affect the suction stress of the compacted loess samples at a microscopic scale.

3.3.1 SEM observations

As an example, the SEM photos of the samples (Figure 5) when the dry density was 1.45g/cm^3 and 1.65g/cm^3 were used to analyze the influence of drying-wetting cycles on loess microstructure. The figure illustrates that there are inter- and intra-aggregate pores in the compacted loess sample. This double pore structure is caused by compaction under a lower than optimal moisture content (Delage et al. 1996). After three dry and wet cycles, the particle and the contact types of the compacted loess changed to varying degrees. The number of surface contacts between particles decreased, with more round particles and point contacts appearing, and the numbers of pores between particles increased. Among them, when the dry density was 1.65g/cm^3, the change in sample microstructure was the most significant, and when the dry density was 1.45g/cm^3, the change in microstructure was relatively small.

The pore type of the 1.45g/cm^3 dry density samples did not change significantly after the drying-wetting cycles, but the proportion of inter-aggregate pores in the overall microstructure

increased, indicating that the drying-wetting cycles would destroy the structural integrity of the compacted loess. Other indicators of microstructure changed little among the three dry density samples, which was consistent with the finding that the suction stress of the 1.45g/cm^3 dry density loess sample had a small decrease in amplitude after drying and wetting cycles (Figure 4b).

For the loess samples with a dry density of 1.65g/cm^3, the samples had a large size differential and consisted of large and small particles before the drying-wetting cycles. The particles were mainly bonded together in the form of face contact with poor pore connectivity. However, after the wetting and drying cycle, the particle size of the sample decreased and was more uniform. The contact form between particles changed to point contact with more apparent particle contours and greater apparent porosity. The change of particle contact form indicated that water dissolved cement during the wetting and drying cycle, which connected some small and medium-sized pores into macropores (Hu et al. 2020), increasing the soil porosity ratio and the volume of macropores. At the same time, due to irreversible van der Waals forces, the size of soil aggregates increased after the wetting-drying cycle, which made clay closer to the aggregates and created larger aggregates (Day and Robert 1994). The increase of aggregates means that the specific surface area decreased.

In general, the drying-wetting cycles changed the structural characteristics and pore size of the samples. After the drying-wetting cycles, a large discontinuous pore space was formed inside the compacted loess sample. On the one hand, air entered the larger pores more easily, but the discontinuous pore space obstructed the water flow channels. Under the same matrix suction, it was easier to maintain a high saturation, and the thicker the hydration film, the weaker the interaction force between the particles and the smaller the suction stress. In addition, the larger the specific surface area, the stronger the adsorption ability of loess particles between the water-holding capacity of soil and soil particles (Frydman 2009). After the drying-wetting cycles, the specific surface area of the compacted loess sample particles and the water-holding capacity of the loess sample decreased, showing that the slope of the SWCC gradually became steeper (Figure 3), and the suction stress was reduced compared with that before the wet-dry cycle, which was manifested as the downward shift of SSCC (Figure 4).

Fig.5 should be here

3.3.2 NMR analysis

The relaxation time (T_2) distribution curve of the compacted loess sample was obtained through the nuclear magnetic resonance experiment, and the pore size distribution curve of the loess sample before and after different degrees of compaction and drying-wetting cycles was obtained by using equation (1) (Figure 6).

Fig.6 should be here

Before and after the drying-wetting cycles, the pore diameter of the compacted loess showed a typical bimodal distribution. This pore distribution state is consistent with the results of scanning electron microscopy. That is, the pores of the loess sample can be mainly classified as macroscopic pores that are a series of inter-aggregate spaces, while the microscopic pores are a series of intra-aggregate spaces (Ng et al. 2019). As dry density increased across the three samples, the first peak of the pore size distribution curve remained consistent. The dominant diameter of the intra-aggregate pores remained at 0.4μm for all samples, indicating that compaction did not significantly impact this part of the pore. The second peak point of the pore

diameter distribution curve, i.e., the inter-aggregate pore, accounts for the largest proportion of the soil. This is defined as the dominant pore diameter of soil in this study. The dominant pore sizes of the loess samples with dry densities of 1.45, 1.55, and 1.65g/cm^3 were 24, 9.4, and 8.7μm, respectively. The diameter of the dominant pores inside the soil decreased as dry density increased. In addition, the dominant pore diameter of the loess samples with the same dry density increased to varying degrees after the drying-wetting cycles. The dominant diameters of samples with dry densities of 1.45, 1.55, and 1.65g/cm^3 increased to 29.7, 24.3, and 23.5μm, respectively, after wetting and drying. Compared with the other two dry densities, the pores of the 1.45g/cm^3 sample were least affected by the drying-wetting cycles, which may be one reason that this sample also showed the smallest change in absorption stress before and after the wetting cycle.

In order to facilitate the study of the relationship between pore size and suction stress of compacted loess, the Young-Laplace equation (Equation 5) (Washburn and E. 1921) was used to convert pore size into equivalent matric suction so as to better explain the micro-structural mechanism of the effect of drying-wetting cycles on suction stress.

$$\psi = \frac{2T_s \cos a}{r} \tag{5}$$

In the formula, T_s is the surface tension coefficient of the ice-water interface when the temperature is 30°C, T_s=71.42 kN/m (Lu and Likos 2004), and a is the contact angle between soil particles and pore water, which is generally 0°.

Taking the 1.55g/cm^3 loess sample as an example, the dominant pore diameter before the drying-wetting cycles was 9.4μm and the corresponding matrix suction was 15.2kPa, which is almost the same as the AEV (that is, the SSCC inflection point). This fact means that the equivalent matrix suction or air intake value can be used as a threshold value to divide the SSCC into two sections: in the first section (0-15.2kPa), the matrix suction corresponds to the large pores in the compacted loess sample (that is, the inter-aggregate pores). In this pore diameter range or matrix suction range, the suction stress of sample increases sharply with the increase of the matrix suction; in the second section (>15.2kPa), the matrix suction corresponds to the small pores in the compacted loess sample (that is, the intra-aggregate pores), in this pore diameter range or within the range of matrix suction, SSCC changes from steep to slow, and tends to be constant. This rule is still consistent for the sample after the drying-wetting cycles, or when the dominant pore diameter was 24.3 μm and the equivalent matrix suction was 5.87 kPa. This finding shows that for small pores, there was a subtle change of suction stress with matrix suction, while for large pores, the change of suction stress with matrix suction is strong. The SSCC of the compacted loess was closely related to the change of the inter-aggregate pores or the diameter of the dominant pores, while the influence of the intra-aggregate pores was relatively weak. The more obvious the influence of the drying-wetting cycles on the diameter of the dominant pore, the stronger the corresponding change in suction stress. This also explains the significant change in the dominant pore diameter of the 1.65g/cm^3 dry density loess sample after the drying-wetting cycles, followed by smaller changes in the 1.55 and 1.45g/cm^3 samples, while the corresponding change range of the suction stress characteristic curve also decreased sequentially.

3.4 Suction stress calculation model based on PSD parameters

Presently, the suction stress of loess is calculated most commonly based on the relevant

parameters of SWCC. However, SWCC testing is time-consuming, and the above analysis showed that the PSD based on the compacted loess sample can also analyze the change mechanism of suction stress during drying-wetting cycles. Therefore, this paper proposes a new method to calculate the suction stress based on the relevant parameters of the loess PSD.

Since the SWCC of the loess sample is an inverted "S" curve and the cumulative pore size distribution curve of the sample is also an "S" shape, the VG model was modified to fit the cumulative pore size distribution curve.

Using pore diameter instead of matrix suction and pore volume instead of water content, the VG model can be modified as:

$$\mathrm{V}(d) = V_r + \frac{V_s - V_r}{[1 + (b/d)^c]^{1-\frac{1}{c}}} \tag{6}$$

where d is pore diameter (μm); $V(d)$ is pore volume with a pore diameter smaller than d (mm^3/g); V_s is total pore volume (mm^3/g); V_r is residual pore volume (mm^3/g); and b and c are fitting parameters.

Through regression analysis, we found that when the residual pore volume V_r is 0, the correlation coefficient of the fitted curve is higher. Therefore, without changing other fitting parameters and considering V_r=0, formula (6) can be modified as:

$$\mathrm{V}(d) = \frac{V_s}{[1 + (b/d)^c]^{1-\frac{1}{c}}} \tag{7}$$

According to the PSD data of the loess sample obtained from the NMR test, the cumulative pore size distribution curve and fitted parameters of the sample obtained by formula (7) are shown in Figure 7 and Table 3, respectively.

Fig.7 should be here

Table 3 should be here

The correlation coefficients R^2 were all greater than 0.99, indicating that the fitting effect was excellent, and also that formula (7) is suitable for the cumulative PSD curve.

Considering the high degree of similarity between SWCC and the cumulative PSD curve in shape and the close relationship between the two, we established the correlation between the parameters a and n from SWCC and the parameters b and c from the cumulative PSD curve. Figure 8 shows that there is a highly linear correlation between the fitted parameters.

Fig.8 should be here

Therefore, the PSD parameters b and c can be used to express the SWCC parameters a and n by means of equations (8) ~ (9).

$$a = 0.0018b - 0.0025 \tag{8}$$

$$n = 1.5041c - 1.0463 \tag{9}$$

By substituting Equations (8) ~ (9) into Equation (3), the suction stress calculation formula (10) based on PSD parameters can be obtained. By using this formula, the suction stress of the corresponding matric suction can be calculated only by obtaining the pore diameter distribution curve of the soil sample. Compared with the traditional method, it is both faster and simpler.

$$\sigma^s = -\psi \left\{ \frac{1}{1 + [(0.0018b - 0.0025)\psi]^{1.5041c-1.0463}} \right\}^{1-\frac{1}{1.5041c-1.0463}} \tag{10}$$

To verify the applicability and accuracy of the suction stress calculation model (10) proposed based on the PSD index, the same type of loess was used in this study, and compacted samples with a moisture content of 10% and a dry density of 1.60g/cm^3 were prepared according to the same method. Some of these samples were subjected to three dry and wet cycles. After testing their SWCC, based on the SWCC parameters, the suction stress before and after the drying-wetting cycles was calculated, and then the matrix suction and suction stress data were fitted using equation (10). The fitted results are shown in Figure 9 with a correlation coefficient of 0.962. This shows that the suction stress calculation model based on the PSD index proposed in this study is a reasonable and feasible estimation method for the loess in the Yan'an area.

Fig.9 should be here

The conversion between matrix suction, suction stress, and PSD parameters demonstrated that SWCC and SSCC are significantly affected by soil microstructure and further verifies that the variation of suction stress before and after the wetting-drying cycle can be attributed to changes in pore structure, which is consistent with SEM and NMR test results.

4. Conclusion

In this study, the influence of drying-wetting cycles on the suction stress of compacted loess was studied using the filter paper method for the first time. SEM and NMR tests were conducted on the samples before and after the drying-wetting cycles to analyze the relationship between the evolution of the microstructure of samples before and after the drying-wetting cycles and SSCC. The main conclusions are as follows:

1. After the drying-wetting cycles, the water-holding capacity of compacted loess decreased, and the interaction forces between the particle layers under the same matrix suction, that is, the suction stress, decreased. The greater the degree of compaction of the sample, the more significant the influence of drying-wetting cycles on the change of suction stress.

2. The drying-wetting cycles did not change the particle composition of the compacted loess. The SSCC before and after the drying-wetting cycles was bounded by the air intake value, which showed nonlinearity and belonged to the typical silty soil form.

3. The influence of drying-wetting cycles on the suction stress of compacted loess samples was specifically reflected in the changes in sample microstructure: (1) The samples subjected to drying-wetting cycles were more likely to form larger pores with a greater distance between particles, reducing the van der Waals force between particles. (2) The specific surface area of soil particles was reduced, decreasing the adsorption capacity between particles; (3) A thick hydration film can be formed between particles and water, weakening the interaction force between particles and reducing the suction stress under the same matric suction force. The change of SSCC with the drying-wetting cycles reflects the comprehensive influence of the drying-wetting cycles on the interaction force between particles.

4. The most significant changes in suction stress with matrix suction are concentrated in the dominant pore range of the soil (that is, the inter-aggregate pores), and the change is small in the small pores range (that is, the intra-aggregate pores). The drying-wetting cycles increase the diameter of the dominant pores in compacted loess, and the larger the diameter of the dominant pores, the smaller the suction stress under the same matrix suction. Therefore, the change mechanism of the two is consistent with the action of the drying-wetting cycles.

5. There is an excellent correlation between PSD and SWCC before and after the drying-

wetting cycles in compacted loess. Based on this phenomenon, this paper proposes a new method for calculating suction stress based on PSD parameters. This method can calculate suction stress by testing the pore size distribution curve of compacted loess, which is more convenient and faster than traditional methods.

Acknowledgment

The authors gratefully acknowledge the Second Tibetan Plateau Scientific Expedition and Research (STEP) program (Grant No. 2019QZKK0905), Key Program of the National Natural Science Foundation of China (Grant no. 41931285), and the key research and development program of Shaanxi Province (Grant no. 2019ZDLSF05-07).

References

Al-Homoud AS, Basma AA, Husein Malkawi AI, Al Bashabsheh MA (1995) Cyclic Swelling Behavior of Clays Journal of Geotechnical Engineering 121:562-565 doi:10.1061/(ASCE)0733-9410(1995)121:7(562)

ASTM (2006) Annual Book of ASTM Standards. ASTM International, West Conshohocken, Pa.

ASTM (2013) Annual Book of ASTM Standards. ASTM International, West Conshohocken, Pa.

Azizi A, Musso G, Jommi C (2019) Effects of repeated hydraulic loads on microstructure and hydraulic behaviour of a compacted clayey silt Canadian Geotechnical Journal doi:10.1139/cgj-2018-0505

Bishop AW (1959) The Principle of Effective Stress Teknisk Ukeblad 39

Bishop AW, Blight GE (1963) Some Aspects of Effective Stress in Saturated and Partly Saturated Soils Géotechnique 13:177-197 doi:10.1680/geot.1963.13.3.177

Burger CA, Shackelford CD (2001) Evaluating dual porosity of pelletized diatomaceous earth using bimodal soil-water characteristic curve functions Canadian Geotechnical Journal 38:53-66 doi:10.1139/cgj-38-1-53

Collins BD, Znidarcic D (2004) Stability Analyses of Rainfall Induced Landslides Journal of Geotechnical & Geoenvironmental Engineering 130:362-372 doi:10.1061/(ASCE)1090-0241(2004)130:4(362)

Day and Robert W (1994) Swell-Shrink Behavior of Compacted Clay Journal of Geotechnical Engineering 120:618-623 doi:10.1061/(ASCE)0733-9410(1994)120:3(618)

Delage P, Audiguier M, Cui YJ, Howat MD (1996) Microstructure of a compacted silt Canadian Geotechnical Journal 33:150-158 doi:10.1139/t96-030

Derbyshire E (2000) Landslides in the thick loess terrain of North-West China. Wiley

Feng SJ, Du FL, Shi ZM, Shui WH, Tan K (2015) Field study on the reinforcement of collapsible loess using dynamic compaction Engineering Geology 185:105-115 doi:10.1016/j.enggeo.2014.12.006

Fredlund, Rahardjo DG (1993) Soil mechanics for unsaturated soils. Wiley,

Fredlund DG, Morgenstern NR (1978) Stress state variables for unsaturated soils Journal of the Geotechnical Engineering Division 103

Fredlund DG, Xing A (1994) Equations for the soil-water characteristic curve Canadian Geotechnical Journal 31:521-532 doi:10.1139/t94-061

Frydman RBS (2009) Unsaturated soil mechanics Critical review of physical foundations

Engineering Geology 106:26-39 doi:10.1016/j.enggeo.2009.02.010

Genuchten V, Th. M (1980) A closed-form equation for predicting the hydraulic conductivity of unsaturated soils Soil Science Society of America Journal 44:892-898 doi:10.2136/sssaj1980.03615995004400050002x

Hu CM, Yuan YL, Mei Y, Wang XY, Liu Z (2020) Comprehensive strength deterioration model of compacted loess exposed to drying-wetting cycles Bulletin of Engineering Geology & the Environment 79:383-398 doi:10.1007/s10064-019-01561-8

Jiang Y, Chen W, Wang G, Sun G, Zhang F (2016) Influence of initial dry density and water content on the soil–water characteristic curve and suction stress of a reconstituted loess soil Bulletin of Engineering Geology & the Environment 76 doi:10.1007/s10064-016-0899-x

Khalili N, Khabbaz MH (2015) A unique relationship for χ for the determination of the shear strength of unsaturated soils Géotechnique 52:477-478 doi:10.1680/geot.51.5.477.39975

Kleinberg, R. L (2003) Deep sea NMR: Methane hydrate growth habit in porous media and its relationship to hydraulic permeability, deposit accumulation, and submarine slope stability Journal of Geophysical Research 108:- doi:10.1029/2003JB002389

Kong L, Sayem HM, Tian H (2017) Influence of drying–wetting cycles on soil-water characteristic curve of undisturbed granite residual soils and microstructure mechanism by nuclear magnetic resonance (NMR) spin-spin relaxation time (T2) relaxometry Canadian Geotechnical Journal:cgj-2016-0614 doi:10.1139/cgj-2016-0614

Leong EC, Rahardjo H (1997) Review of Soil-Water Characteristic Curve Equations Journal of Geotechnical & Geoenvironmental Engineering 123:1106-1117 doi:10.1061/(ASCE)1090-0241(1997)123:12(1106)

Li G, Wang F, Ma W, Fortier R, Mu Y, Mao Y, Hou X (2018) Variations in strength and deformation of compacted loess exposed to wetting-drying and freeze-thaw cycles Cold Regions Science & Technology 151:159-167 doi:10.1016/j.coldregions.2018.03.021

Liu TC (2011) Desiccation and cracking behaviour of clay layer from slurry state under wetting–drying cycles Geoderma doi:10.1016/j.geoderma.2011.07.018

Lourenco SDN, Wang GH, Kamai T (2015) Processes in model slopes made of mixtures of wettable and water repellent sand: Implications for the initiation of debris flows in dry slopes Engineering Geology 196:47-58 doi:10.1016/j.enggeo.2015.06.021

Lu N (2004) Profiles of Steady-State Suction Stress in Unsaturated Soils Journal of Geotechnical & Geoenvironmental Engineering 130:1063-1076 doi:10.1061/(ASCE)1090-0241(2004)130:10(1063)

Lu N, Godt JW, Wu DT (2010) A closed-form equation for effective stress in unsaturated soil Water Resources Research 46:n/a-n/a doi:10.1029/2009wr008646

Lu N, Likos WJ (2004) Unsaturated soil mechanics. J. Wiley,

Lu N, Likos WJ (2006) Suction Stress Characteristic Curve for Unsaturated Soil Journal of Geotechnical & Geoenvironmental Engineering 132:131-142 doi:10.1061/(ASCE)1090-0241(2006)132:2(131)

Luo H, Wu F, Chang J, Xu J (2017) Microstructural constraints on geotechnical properties of Malan Loess: A case study from Zhaojiaan landslide in Shaanxi province, China Engineering Geology:S0013795217315879 doi:10.1016/j.enggeo.2017.11.002

Ng CWW, Mu QY, Zhou C (2019) Effects of specimen preparation method on the volume change of clay under cyclic thermal loads Geotechnique 69:146-150

doi:10.1680/jgeot.16.p.293

Ni W-k, Yuan K-z, Lu X-f, Yuan Z-h (2020) Comparison and quantitative analysis of microstructure parameters between original loess and remoulded loess under different wetting-drying cycles Scientific Reports 10 doi:10.1038/s41598-020-62571-1

Oh S, Lu N, Yun KK, Lee SJ, Lee SR (2012) Relationship between the Soil-Water Characteristic Curve and the Suction Stress Characteristic Curve: Experimental Evidence from Residual Soils Journal of Geotechnical & Geoenvironmental Engineering 138:47-57 doi:10.1061/(ASCE)GT.1943-5606.0000564

Oh S, Ning L, Kim TK, Lee YH (2013) Experimental Validation of Suction Stress Characteristic Curve from Nonfailure Triaxial K0 Consolidation Tests Journal of Geotechnical & Geoenvironmental Engineering 139:1490-1503 doi:10.1061/(ASCE)GT.1943-5606.0000880

Peng J, Qi S, Williams A, Dijkstra TA (2018) Preface to the special issue on "Loess engineering properties and loess geohazards" Engineering Geology 236:1-3 doi:10.1016/j.enggeo.2017.11.017

Peng JB, Wang GH, Wang QY, Zhang FY (2017) Shear wave velocity imaging of landslide debris deposited on an erodible bed and possible movement mechanism for a loess landslide in Jingyang, Xi'an, China Landslides 14:1503-1512 doi:10.1007/s10346-017-0827-6

Qin P et al. (2020) An Electrical Resistivity Method of Characterizing Hydromechanical and Structural Properties of Compacted Loess During Constant Rate of Strain Compression Sensors 20 doi:10.3390/s20174783

Schnellmann R, Busslinger M, Schneider HR, Rahardjo H (2010) Effect of rising water table in an unsaturated slope Engineering Geology 114:71-83 doi:10.1016/j.enggeo.2010.04.005

Sommer R, Stoeckle C (2010) Correspondence between the Campbell and van Genuchten Soil-Water-Retention Models Journal of Irrigation & Drainage Engineering 136:559-562 doi:10.1061/(ASCE)IR.1943-4774.0000204

Song JTH (2012) A comparative study of suction stress between sand and silt under unsaturated conditions Engineering Geology doi:10.1016/j.enggeo.2011.10.006

Song YS (2014) Suction stress in unsaturated sand at different relative densities Engineering Geology 176:1-10 doi:10.1016/j.enggeo.2014.04.002

Song YS, Hong S (2020) Effect of clay minerals on the suction stress of unsaturated soils Engineering Geology 269:105571- doi:10.1016/j.enggeo.2020.105571

Tian H, Wei C, Wei H, Yan R, Pan C (2014) An NMR-Based Analysis of Soil–Water Characteristics Applied Magnetic Resonance 45:49-61 doi:10.1007/s00723-013-0496-0

Vanapalli SK, Fredlund DG, Pufahl DE, Clifton AW (1996) Model for the prediction of shear strength with respect to soil suction Canadian Geotech Jour 33:379-392 doi:10.1139/t96-060

Washburn, E. W (1921) Note on a Method of Determining the Distribution of Pore Sizes in a Porous Material Proceedings of the National Academy of Sciences of the United States of America 7:115-116 doi:10.1073/pnas.7.4.115

Xie X, Li P, Hou X, Li T, Zhang G (2020) Microstructure of Compacted Loess and Its Influence on the Soil-Water Characteristic Curve Advances in Materials Science & Engineering 2020:1-12 doi:10.1155/2020/3402607

Zhai Q, Rahardjo H (2012) Determination of soil–water characteristic curve variables Computers & Geotechnics 42:37-43 doi:10.1016/j.compgeo.2011.11.010

Zhang F, Zhao C, Loureno SDN, Dong S, Jiang Y (2020) Factors affecting the soil–water retention curve of Chinese loess Bulletin of Engineering Geology & the Environment doi:10.1007/s10064-020-01959-9

Figures

Fig. 1

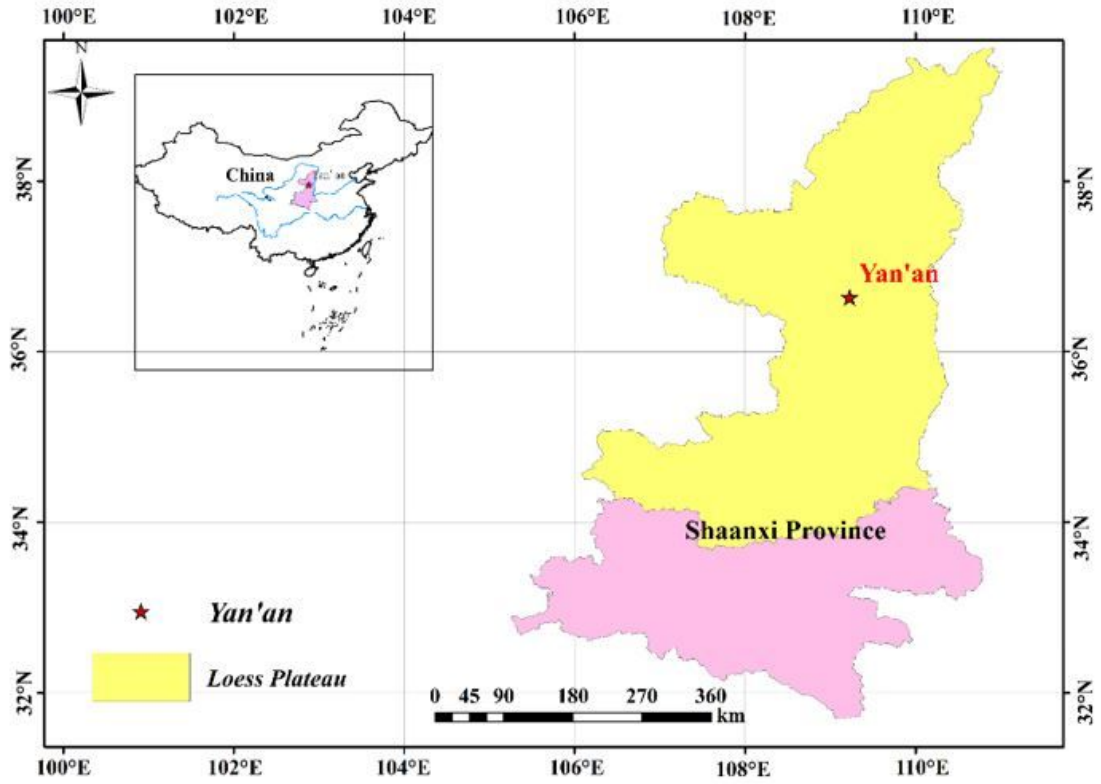

Figure 1

Loess distribution and sampling sites in Shaanxi, China Note: The designations employed and the presentation of the material on this map do not imply the expression of any opinion whatsoever on the part of Research Square concerning the legal status of any country, territory, city or area or of its authorities, or concerning the delimitation of its frontiers or boundaries. This map has been provided by the authors.

Fig. 2

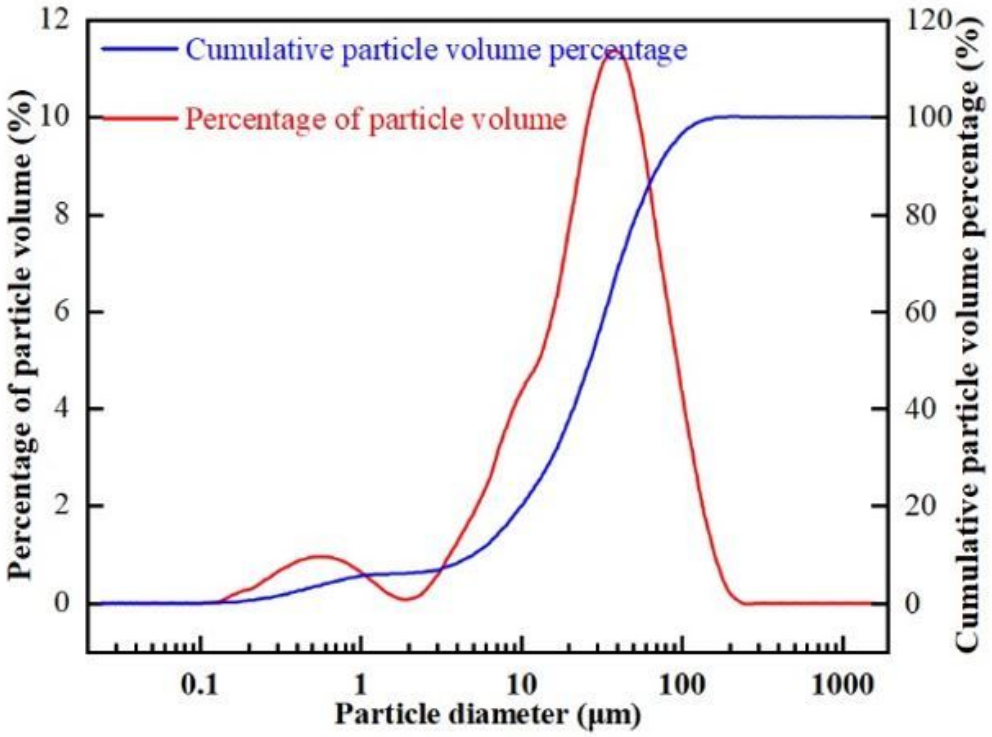

Figure 2

Grain size composition of loess samples

Fig. 3

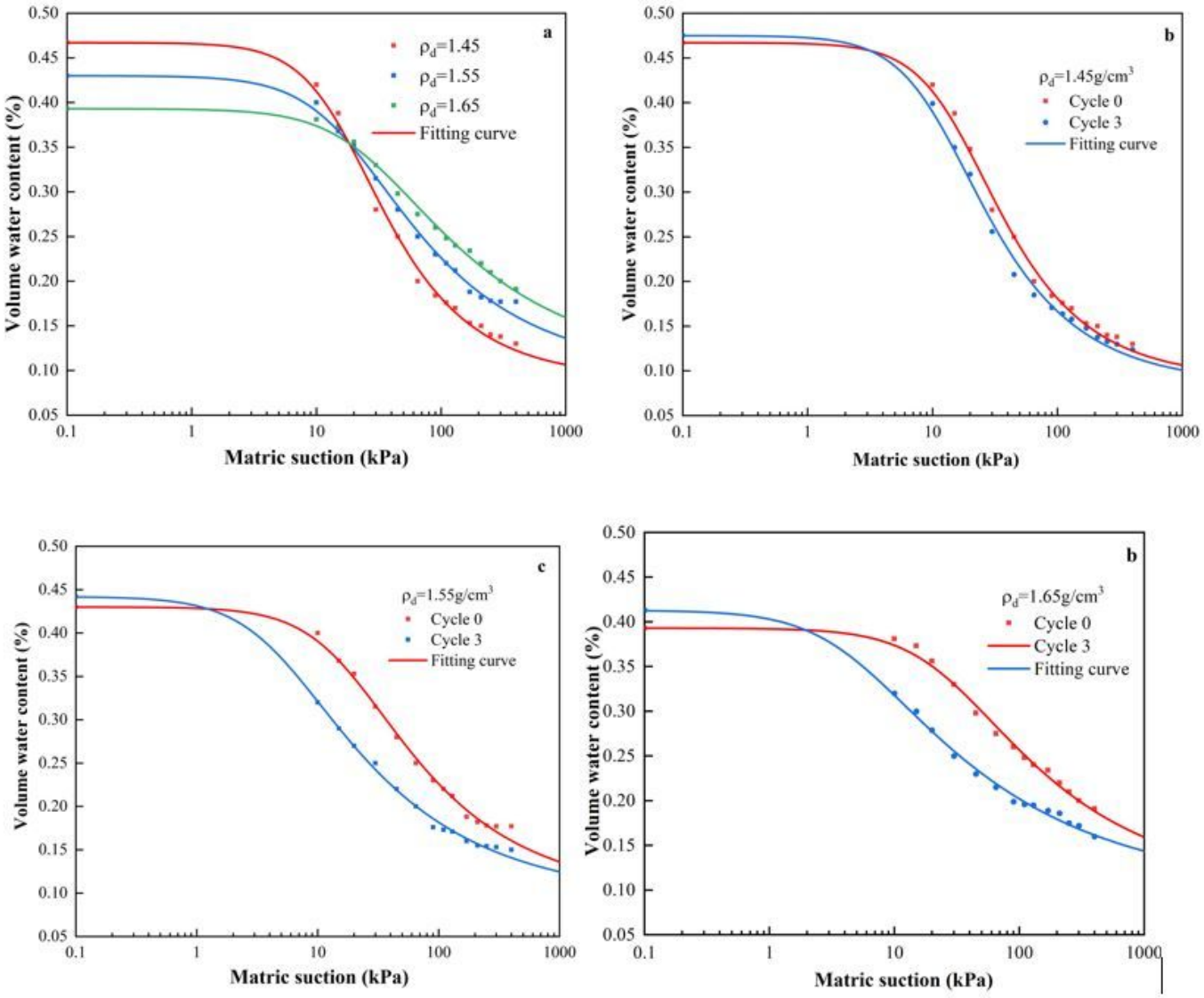

Figure 3

SWCC of compacted loess samples

Fig. 4

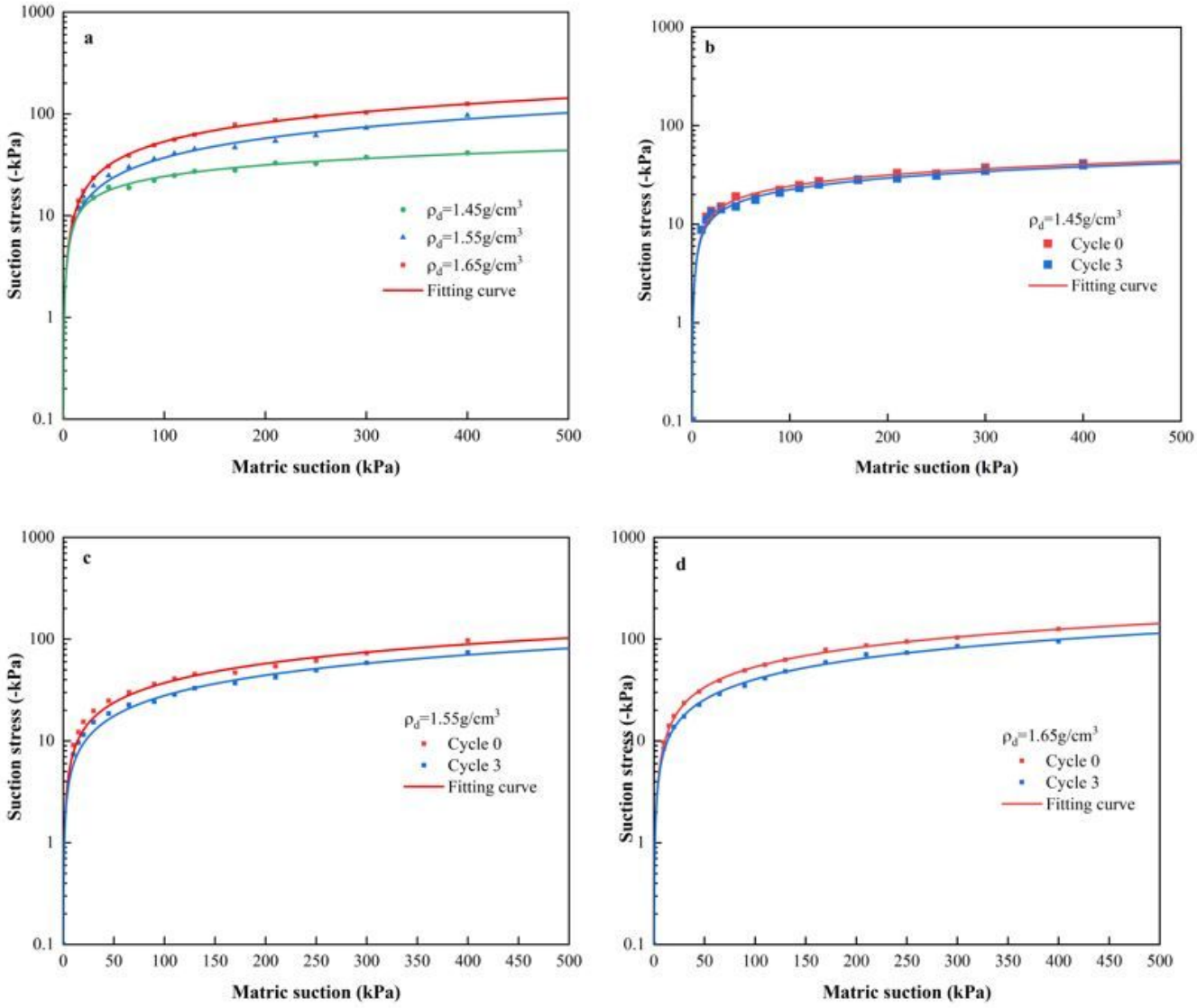

Figure 4

SSCC of compacted loess samples

Fig. 5

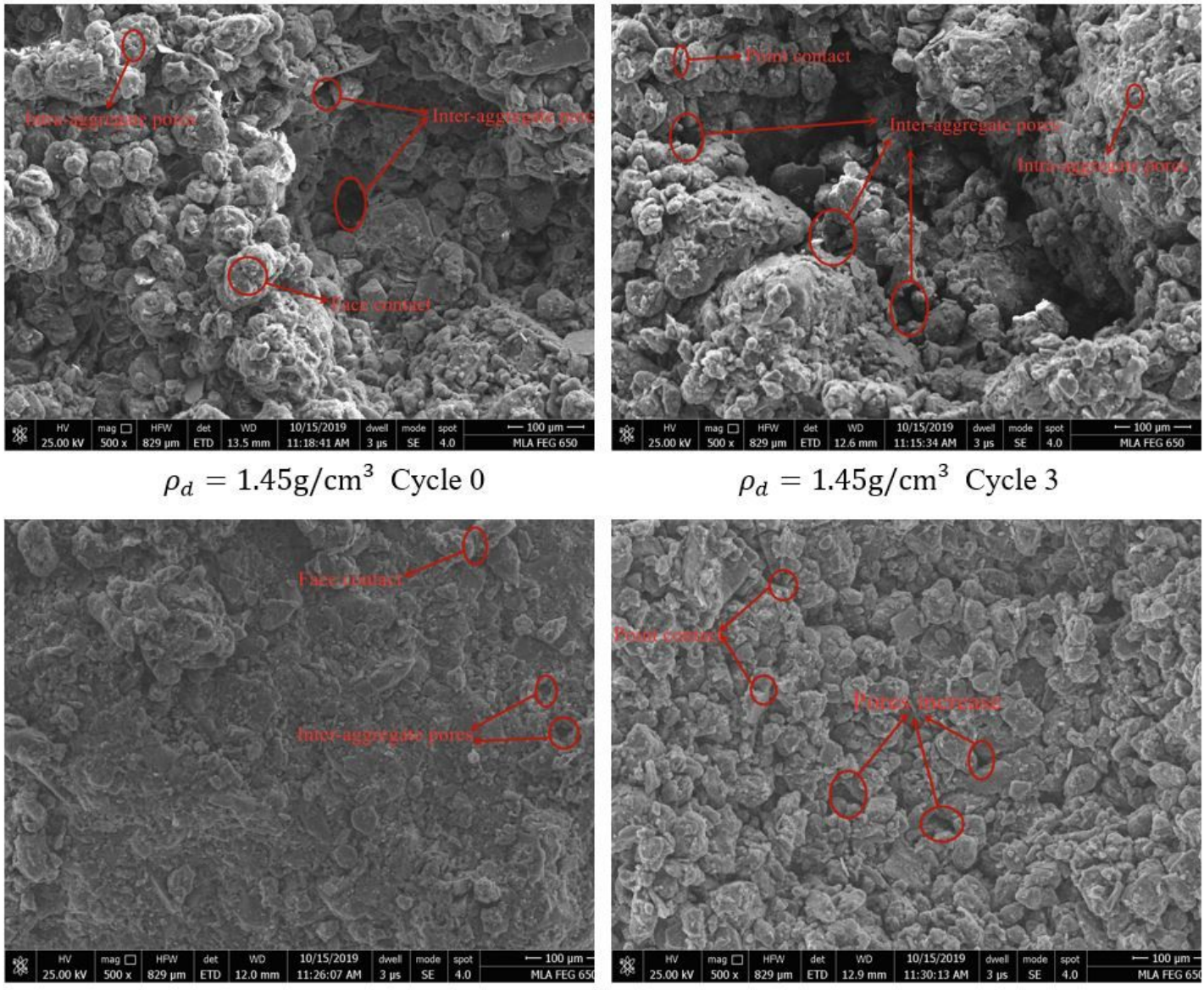

$\rho_d = 1.45\text{g/cm}^3$ Cycle 0

$\rho_d = 1.45\text{g/cm}^3$ Cycle 3

$\rho_d = 1.65\text{g/cm}^3$ Cycle 0

$\rho_d = 1.65\text{g/cm}^3$ Cycle 3

Figure 5

SEM photo of compacted loess samples

Fig. 6

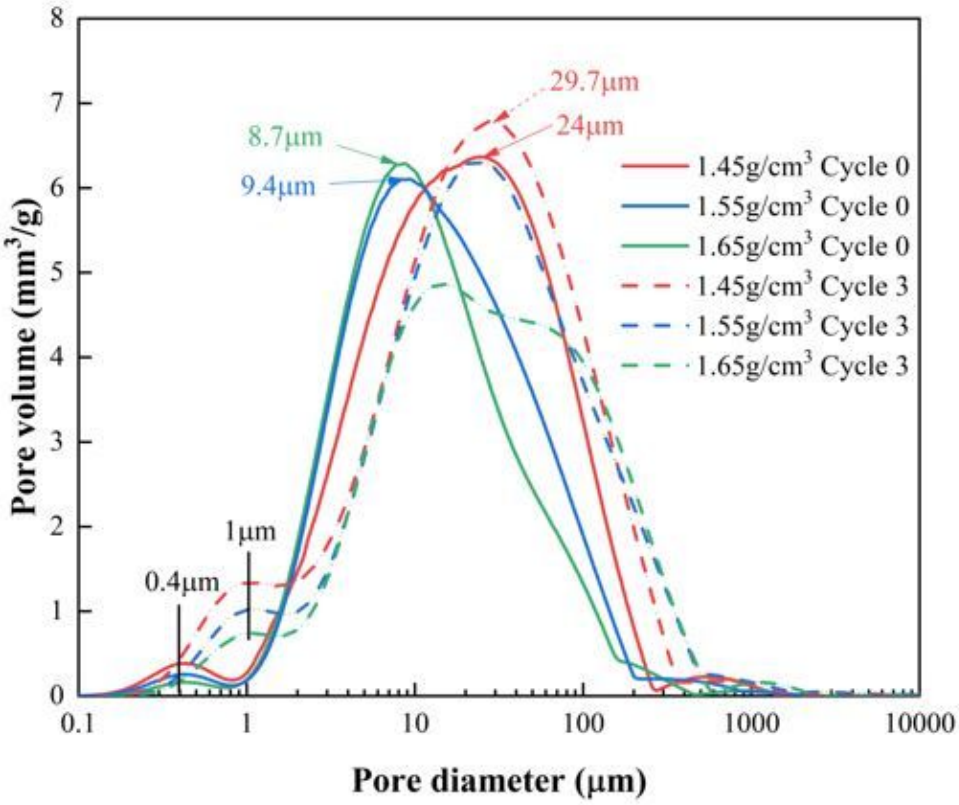

Figure 6

PSD of compacted loess samples

Fig. 7

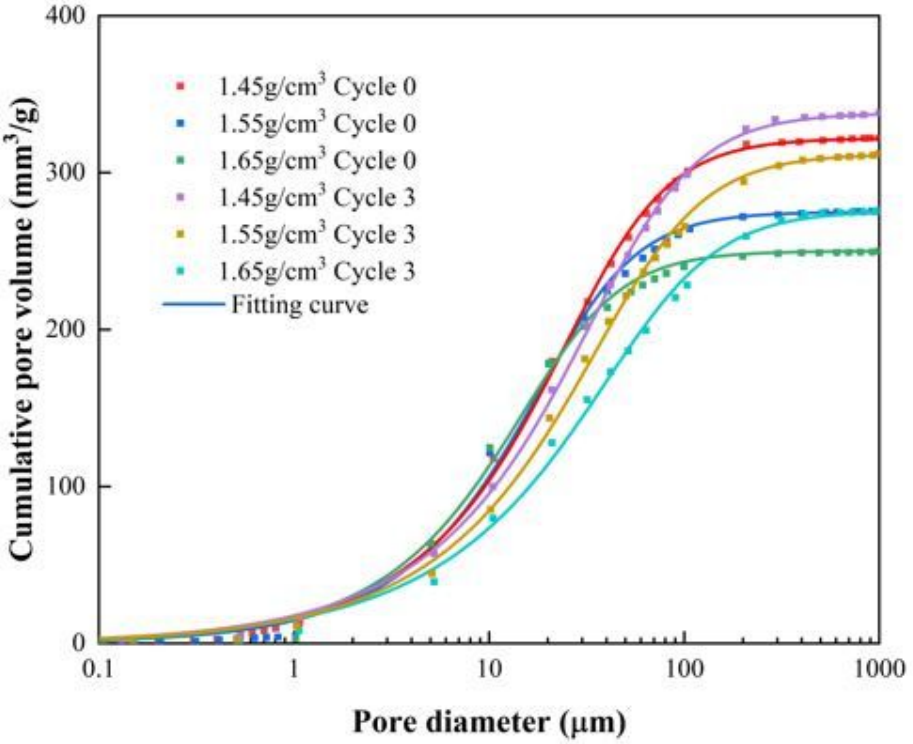

Figure 7

The cumulative PSD fitted curves of samples considering V_r= 0

Fig. 8

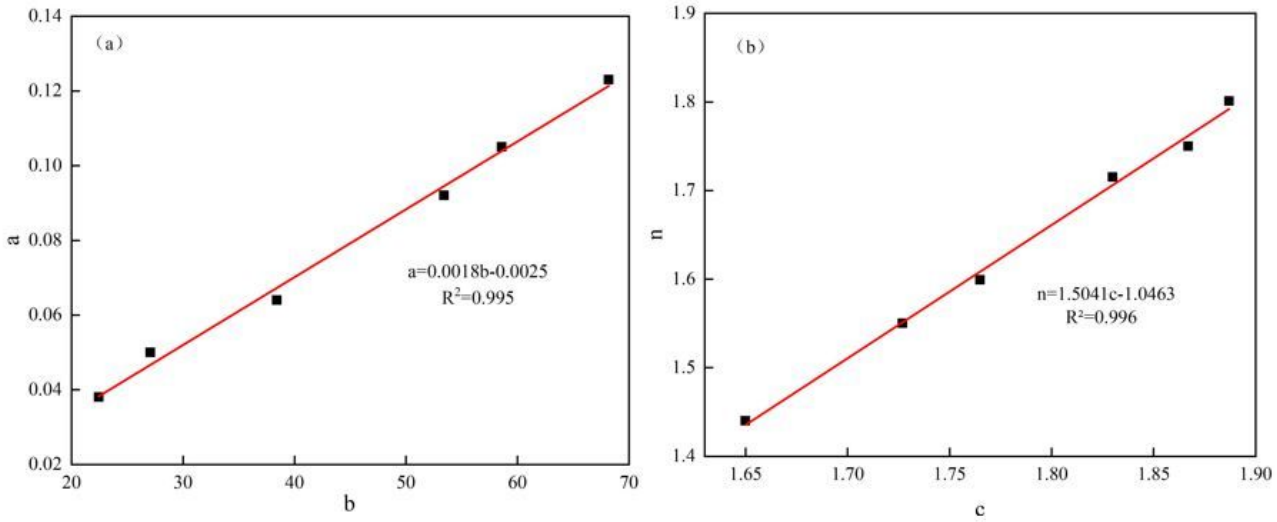

Figure 8

The relationship between fitted parameters

Fig. 9

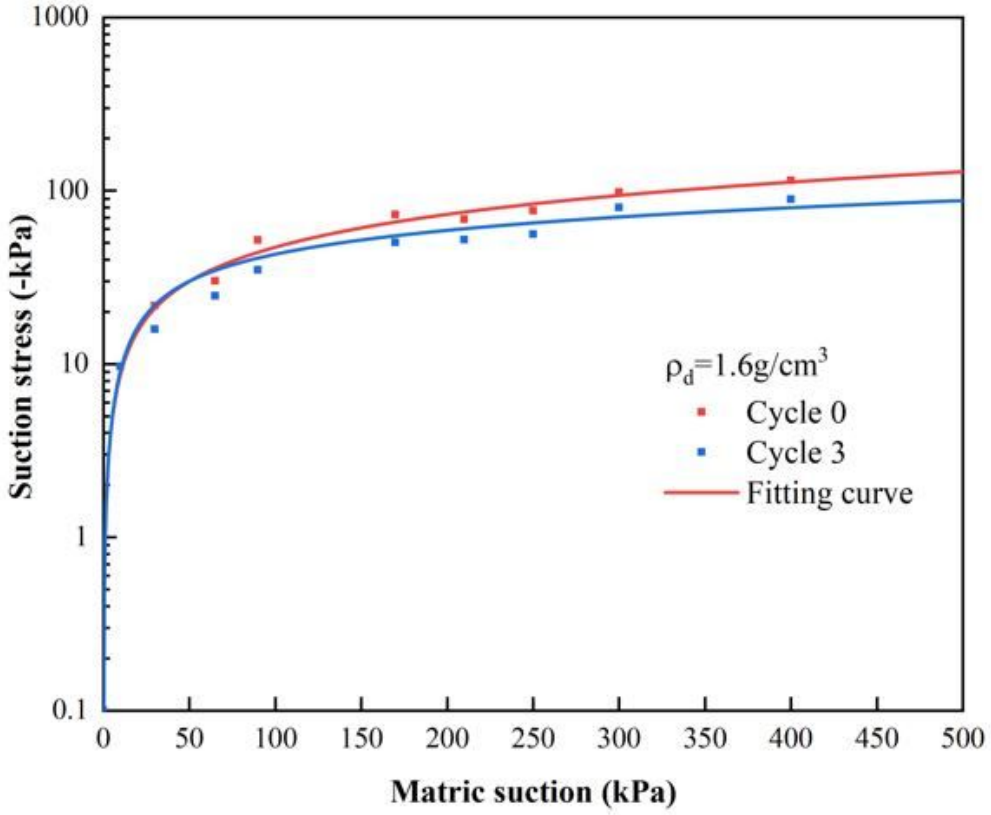

Figure 9

ρ_d=1.6g/cm³ loess sample SSCC fitted by the modified model